Supporting Information

Catalytic oxidation of formaldehyde over a Au@Co_3O_4 nanocomposite catalyst enhanced by visible light: Moisture indispensability and reaction mechanism

Qiuxia Liu[a,b], Yuelong Wang[a,b], Meicheng Wen[a,b], Yunlong Guo[a,b], Yupeng Wei[a,b], Guiying Li[a,b], Taicheng An[a,b],*

[a] *Guangdong Key Laboratory of Environmental Catalysis and Health Risk Control, Guangdong-Hong Kong-Macao Joint Laboratory for Contaminants Exposure and Health, Institute of Environmental Health and Pollution control, Guangdong University of Technology, Guangzhou 510006, China;*

[b] *Guangdong Engineering Technology Research Center for Photocatalytic Technology Integration and Equipment, Guangzhou Key Laboratory of Environmental Catalysis and Pollution Control, School of Environmental Science and Engineering, Guangdong University of Technology, Guangzhou 510006, China.*

Corresponding author: Prof. Taicheng An

Tel: 86-20-39322298; E-mail: antc99@gdut.edu.cn

Text S1. Catalyst synthesis

In order to ensure the objectivity of the control experiment, we prepared TiO_2, Au@TiO_2, Au@Co_3O_4-0.5, Au@Co_3O_4-2 by the same method as Co_3O_4 and Au@Co_3O_4.

TiO_2: 0.142 mL of Titanium isopropoxide solution ($C_{12}H_{28}O_4Ti$, 0.954 g cm^{-3}) was added into 150 mL water (70 °C), and stirred continuously at 15 rpm for 1 min. After that, 9 mL of ammonia solution ($NH_3 \cdot H_2O$, 0.16-0.19 M) was added and stirred continuously at 15 rpm for 22 min (70 °C). After cooling down to room temperature (30 °C), the precipitate was collected by centrifugation (12000 rpm, 5 min), and washed with distilled water (100 mL) and methanol (40 mL). Finally, the obtained black powder (noted as TiO_2) was dried at 70 °C for 12 h. And proved to be amorphous TiO_2 by XRD (**Fig. S11**).

Au@TiO_2: 1260 μL of chloroauric acid solution ($HAuCl_4$, 0.029 M) was mixed with 150 mL water (70 °C), and stirred at 15 rpm for 1 min. Then, 0.142 mL of Titanium isopropoxide solution ($C_{12}H_{28}O_4Ti$, 0.954 g cm^{-3}) was added into the obtained solution, and stirred continuously at 15 rpm for 1 min. After that, 9 mL of ammonia solution ($NH_3 \cdot H_2O$, 0.16-0.19 M) was added and stirred continuously at 15 rpm for 22 min (70 °C). After cooling down to room temperature (30 °C), the precipitate was collected by centrifugation (12000 rpm, 5 min), and washed with distilled water (100 mL) and methanol (40 mL). Finally, the obtained black powder (noted as Au@TiO_2) was dried at 70 °C for 12 h. It mainly contains Au and amorphous TiO_2 was ensured by XRD (**Fig. S11**).

Au@Co_3O_4-0.5, 500 μL of chloroauric acid solution ($HAuCl_4$, 0.029 M) was mixed with 150 mL water (70 °C), and stirred at 15 rpm for 1 min. Then, 4.8 mL of cobalt nitrate solution ($Co(NO_3)_2$, 0.1 M) was added into the obtained solution, and stirred continuously at 15 rpm for 1 min. After that, 9 mL of ammonia solution ($NH_3 \cdot H_2O$, 0.16-0.19 M) was added and stirred continuously at 15 rpm for 22 min (70 °C). After cooling down to room temperature (30 °C), the precipitate was collected by centrifugation (12000 rpm, 5 min), and washed with distilled water (100 mL) and methanol (40 mL). Finally, the obtained black powder (noted as Au@Co_3O_4-0.5) was dried at 70 °C for 12 h. It mainly contains Au and Co_3O_4 was ensured by XRD (**Fig. S11**).

Au@Co_3O_4-2, 2000 μL of chloroauric acid solution ($HAuCl_4$, 0.029 M) was mixed with 150 mL water (70 °C), and stirred at 15 rpm for 1 min. Then, 4.8 mL of cobalt nitrate solution ($Co(NO_3)_2$, 0.1 M) was added into the obtained solution, and stirred continuously at 15 rpm for 1 min. After that, 9 mL of ammonia solution ($NH_3 \cdot H_2O$, 0.16-0.19 M) was added and stirred continuously at 15 rpm for 22 min (70 °C). After cooling down to room temperature (30 °C), the precipitate was collected by centrifugation (12000 rpm, 5 min), and washed with distilled water (100 mL) and methanol (40 mL). Finally, the obtained black powder (noted as Au@Co_3O_4-2) was dried at 70 °C for 12 h. It mainly contains Au and Co_3O_4 was ensured by XRD (**Fig. S11**).

Text S2. Determination of formaldehyde and intermediate byproducts by GC-MS

The tail gas was extracted by solid-phase microextraction and detected by a gas chromatography-mass spectrometry system (GCMS) (Agilent 7890B-5977B) with O-(2,3,4,5,6-Pentafluorobenzyl) hydroxylamine hydrochloride (PFBHA) as derivate reagent, with a DB-5ms capillary column (30 m × 0.25 mm × 0.25 μm). GC temperature program of column was 60 °C for 1 min, rose to 260 °C at 7 °C min^{-1} holding for 1 min. Mass spectra was performed in full scan mode with an m/z range of 30-280, while the temperature of the transfer line was 300 °C, recorded in electron ionization mode at an ion source temperature of 230 °C.

Text S3. Determination of intermediate byproducts by HPLC

Total 10 mg of the catalyst after the catalytic reaction was immersed in 2 ml of deionized water, and filtering it after ultrasonic treatment for 5 min. Then the filtrate was detected by High-performance liquid chromatography (HPLC) (Agilent 1260) with an Athena C18-WP chromatographic column (10 nm, 4.6 × 150 mm, 5 μm). The amount of sample injected each time is 20 μL, 0.02% phosphoric acid solution is used as the mobile phase, the detection wavelength is 210 nm, and the flow rate is 1 mL min^{-1}. Use formic acid solution and sodium bicarbonate solution for qualitative analysis.

All reagents used above were obtained from Aladdin Reagent Co., Ltd. (Shanghai, China) and employed as received without further purification.

Table S1. Overview of the photocatalytic activities in formaldehyde oxidation of various catalysts.

Sample	Weight /g	Concentration /ppm	GHSV /mL g^{-1} h^{-1}	Catalytic conditions	Removal efficiency	Ref.
Au@ Co_3O_4	0.01	75	300000	200 mW/cm^2 Xenon lamp 360 – 850 nm, Dynamic flow, 25 ℃, RH 76%	91.5%: 15 min (dark) 98.7%:15 min (light)	This work
g-C_3N_4	0.1	180		8w fluorescent lamp Chamber	26%： (dark) 57 %: 7h (light)	1
g-C_3N_4/CeO_2	0.1	180		8w fluorescent lamp Chamber	21%: (dark) 70 %: 7h (light)	1
CeO_2	0.1	180		8w fluorescent lamp Chamber	22%: (dark) 63 %: 7h (light)	1
g-C_3N_4/CeO_2	0.1	140		8w fluorescent lamp Chamber	70.0%: 9h (dark) 77.1%: 9 h (light)	2
CeO_2/CN-1:1	0.3	65 ± 5		100 mW/cm^2Xe lamp ≥420 nm, Dynamic flow, RH 60%	52%: 120 min (dark) 100%: 90 min (light)	3
Sn-$CaSn(OH)_6$	0.4	47.8		Uv lamp (365 nm) Dynamic flow,	79.3%: 12min (light)	4
$BiSbO_4$	0.4		150000	Mercury lamp, 300W Dynamic flow,	92.0%: 20min (ligth)	5
CuO/TiO_2	0.1	180		500W Xe lamp Chamber, RH 40%	90.3%: 150min (light)	6
Eu/CeO_2	0.1	500		100W halogen lamp Chamber, 25℃	80.0 %: 120 min (light)	7
CeO_2	0.1	500		100W halogen lamp Chamber, 25℃	18.8 %: 120min (light)	7

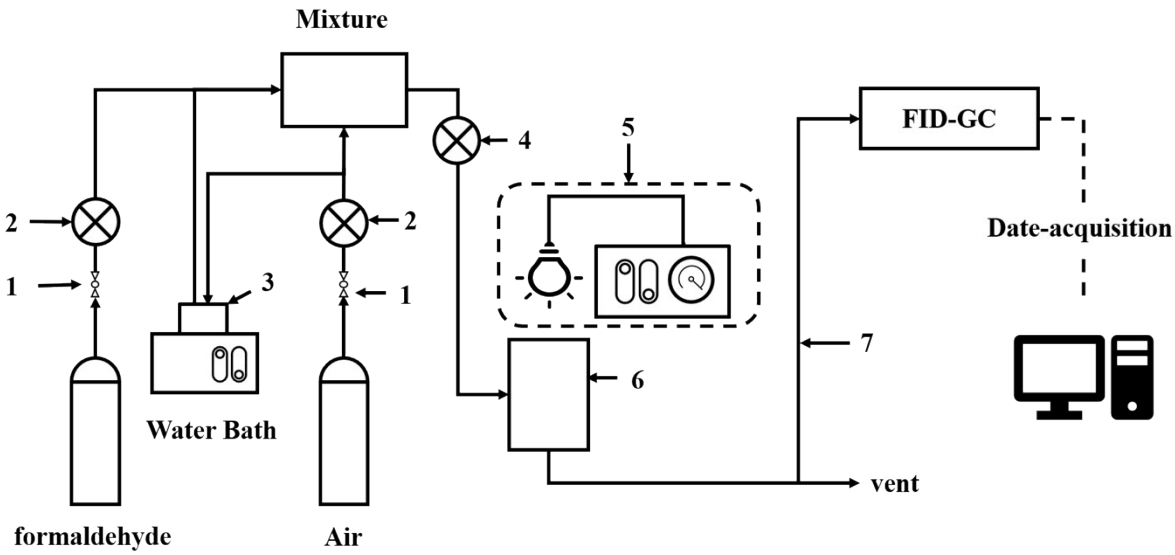

Scheme S1. Schematic of the experimental system. (1) Check value; (2) Pressure gage; (3) Evaporation tank with water; (4) RH gage; (5) Xenon lamp and its power supply; (6) Sample bin; (7) Sample port for gas detection tube.

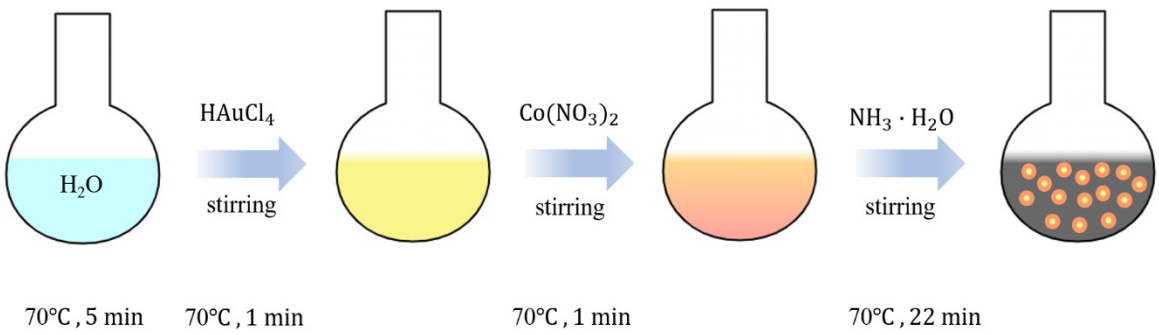

Fig. S1. Schematic of the synthetic route of Au@Co_3O_4 nanocomposite.

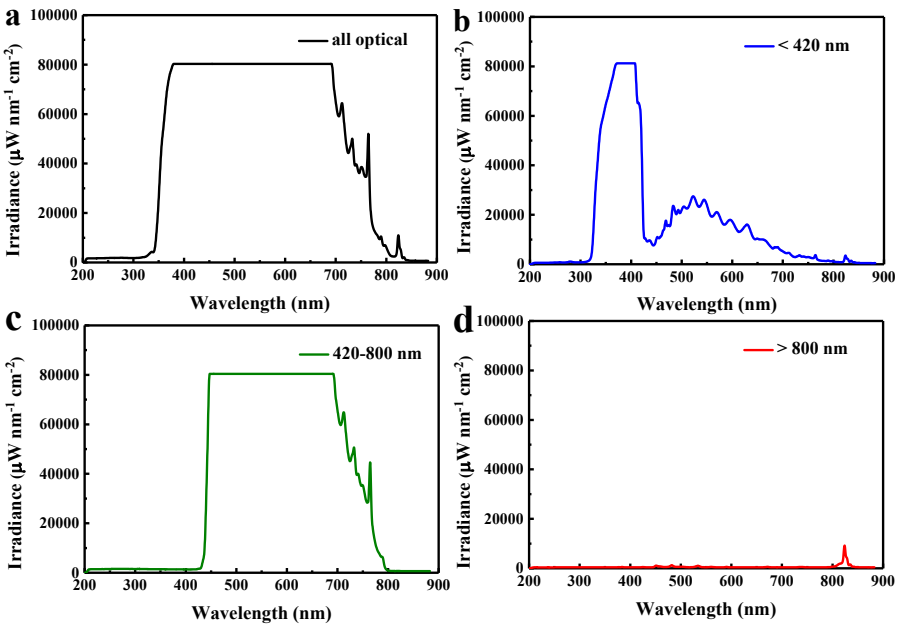

Fig. S2. The spectral range of the xenon lamp: all optical (a), <420 nm (b), 420-800 nm (c), >800 nm (d).

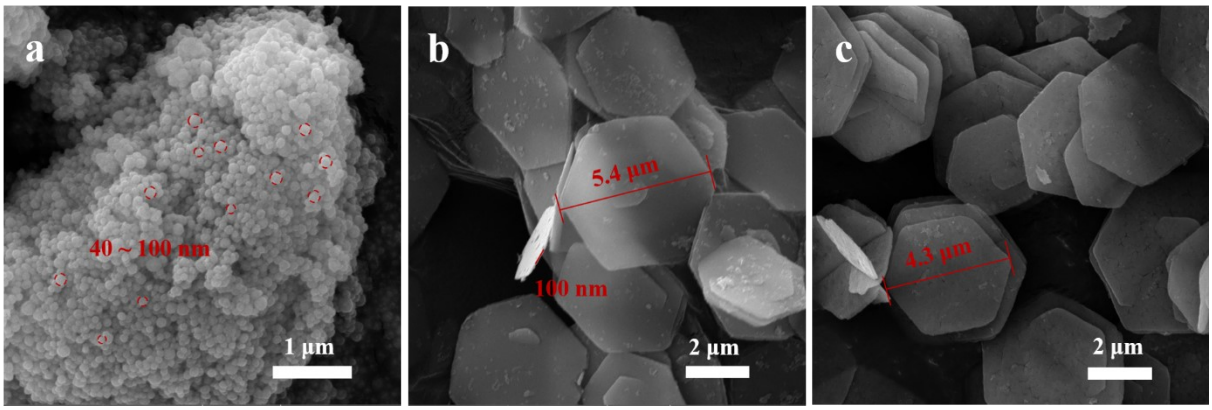

Fig. S3. SEM image of Au@Co_3O_4 nanocomposite (a), $Co(OH)_2$ and prepared Co_3O_4.

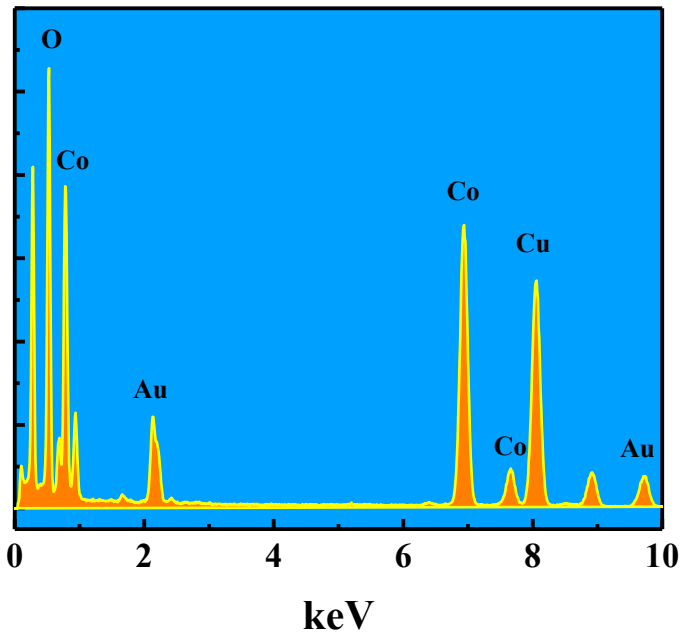

Fig. S4. EDS spectrum map of Au@Co_3O_4 nanocomposite.

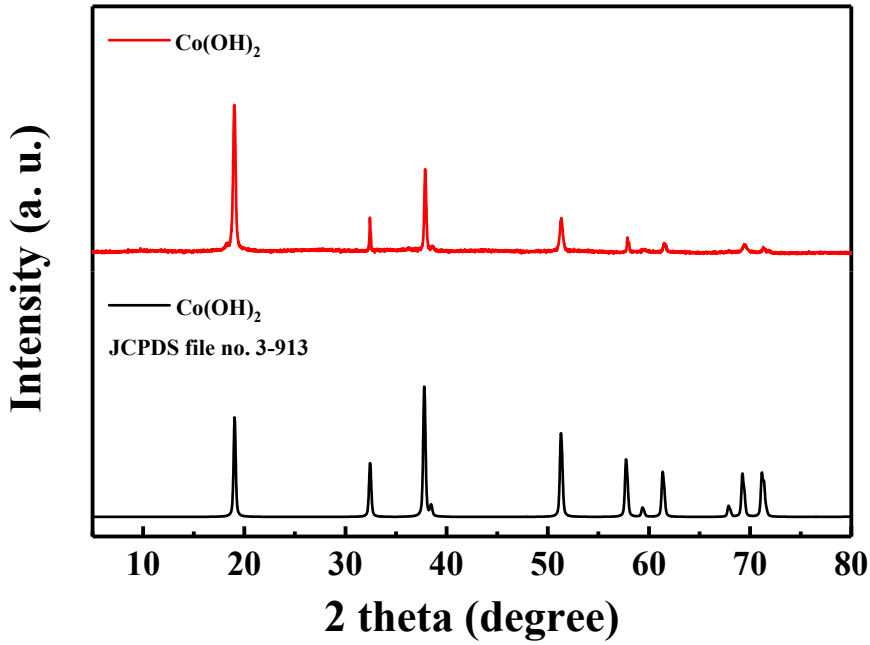

Fig. S5. XRD patterns of $Co(OH)_2$.

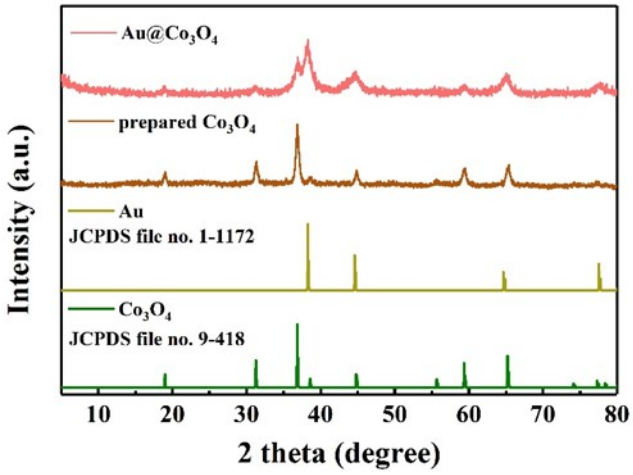

Fig. S6. XRD patterns of prepared Co_3O_4 and Au@Co_3O_4 nanocomposite.

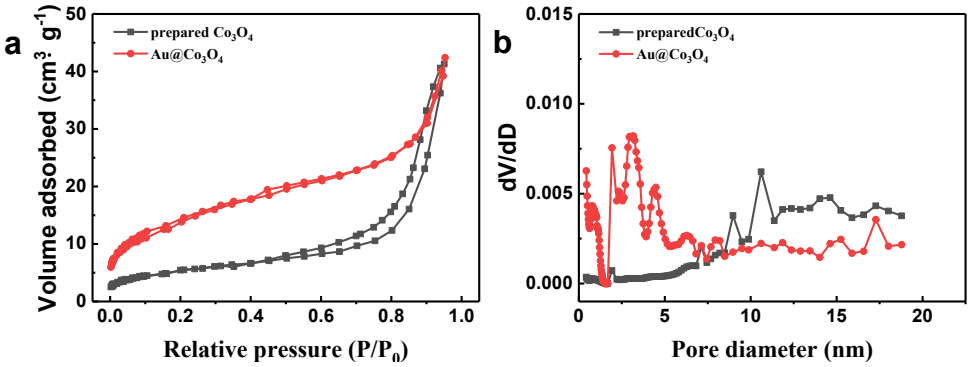

Fig. S7. Nitrogen adsorption-desorption isotherms (a) and the corresponding pore size distributions (b) of prepared Co_3O_4 and Au@Co_3O_4 nanocomposite.

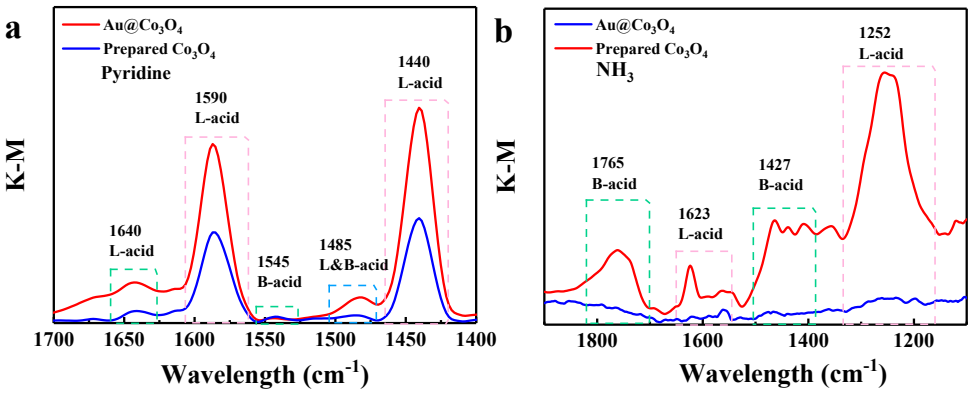

Fig. S8. Pyr-DRIFT (a) and NH_3-DRIFT (b) of prepared Co_3O_4 and Au@Co_3O_4 nanocomposite.

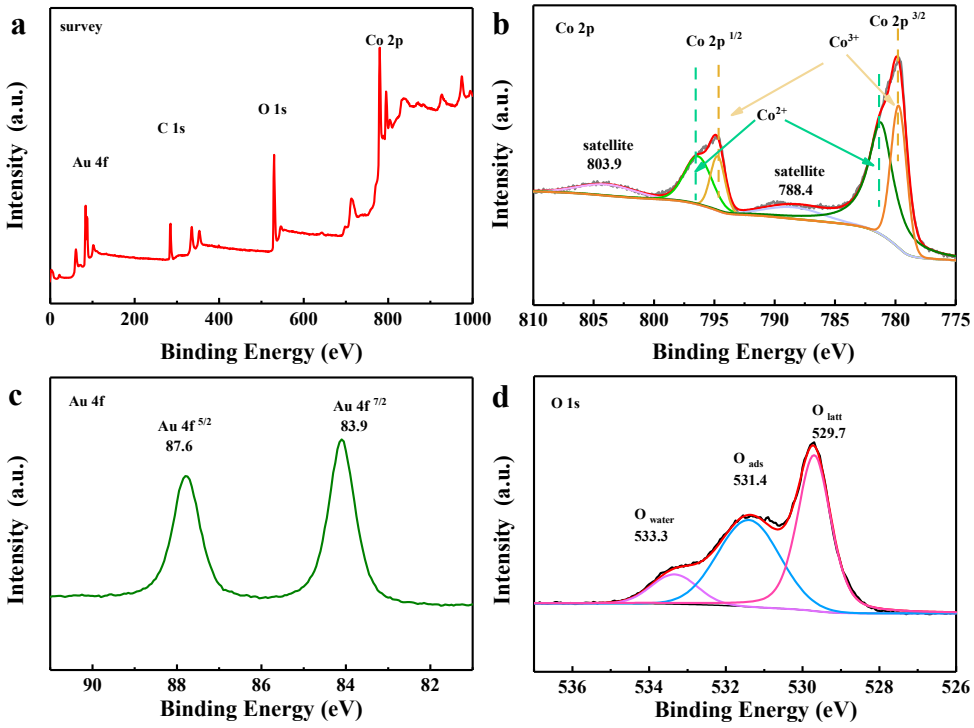

Fig. S9. XPS of Au@Co_3O_4-OTT: survey (**a**), Co 2p (**b**), Au 4f (**c**) and O1 s (**d**).

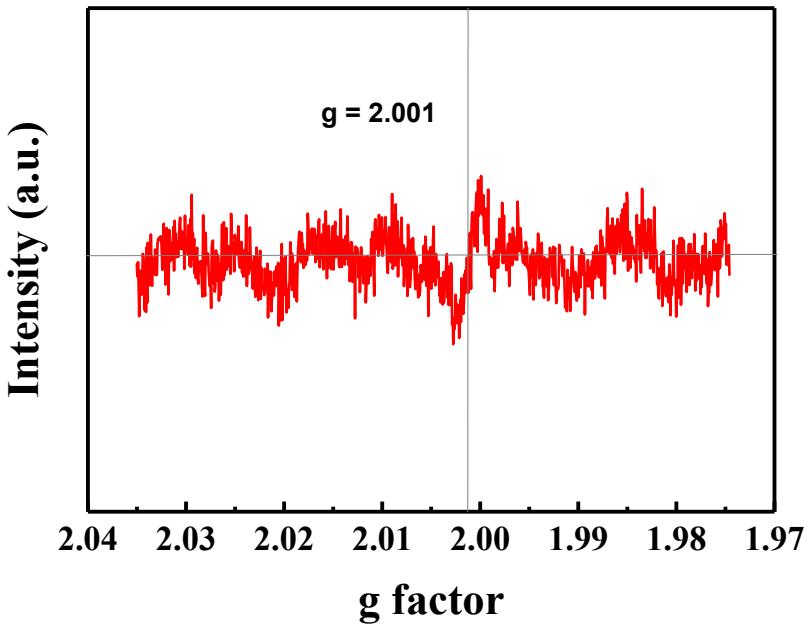

Fig. S10. ESR of Au@Co_3O_4 nanocomposition.

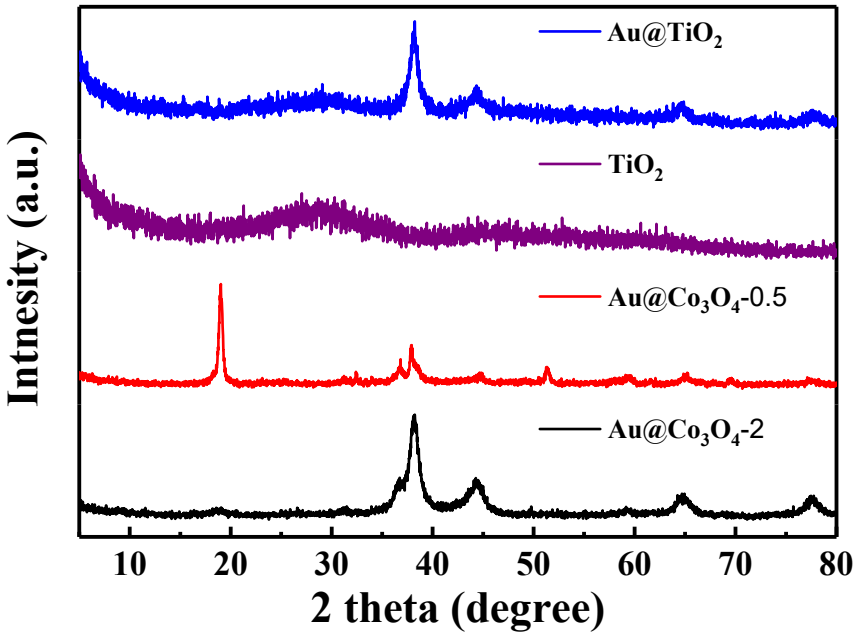

Fig. S11. XRD patterns of TiO_2, Au@TiO_2, Au@Co_3O_4-0.5 and Au@Co_3O_4-2.

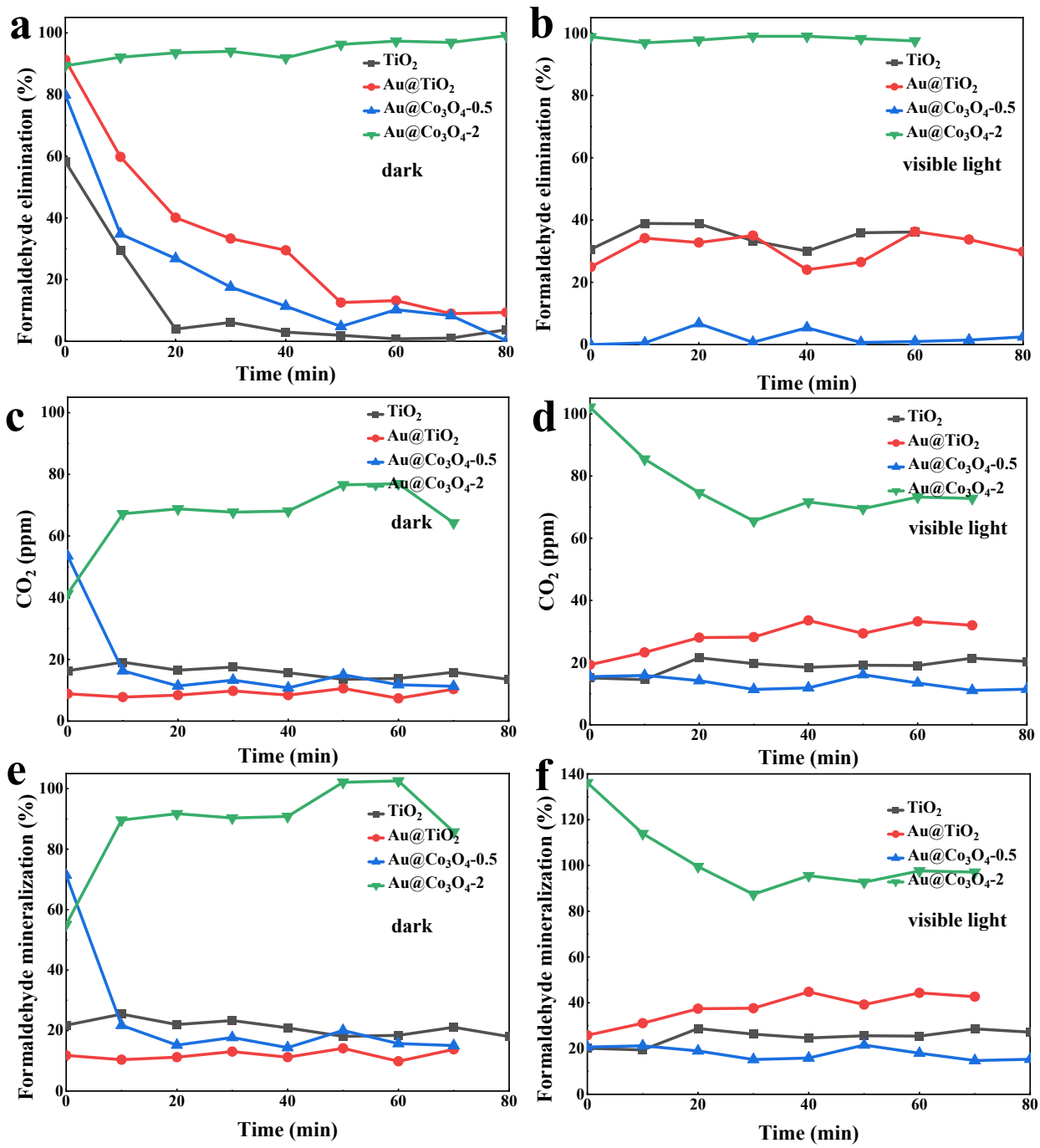

Fig. S12. Control experiment: formaldehyde elimination efficiency (a, b), CO_2 concentration (c, d) and formaldehyde mineralization (e, f) of TiO_2, Au@TiO_2, Au@Co_3O_4-0.5, Au@Co_3O_4-2 in the dark and visible-light irradiation (RH: 45%) in a flow of formaldehyde (75 ppm) at GHSV of 300000 mL h^{-1} g^{-1} (30 ^{o}C, 300 W Xenon lamp).

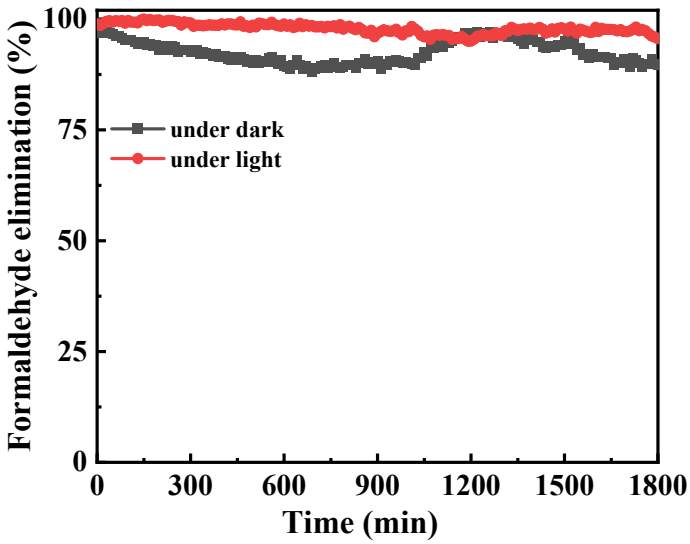

Fig. S13. Formaldehyde elimination efficiency both in the dark and visible-light irradiation at RH 45% in a flow of formaldehyde (75 ppm) at GHSV of 300000 mL h^{-1} g^{-1} (30 ^{o}C, 300 W Xenon lamp).

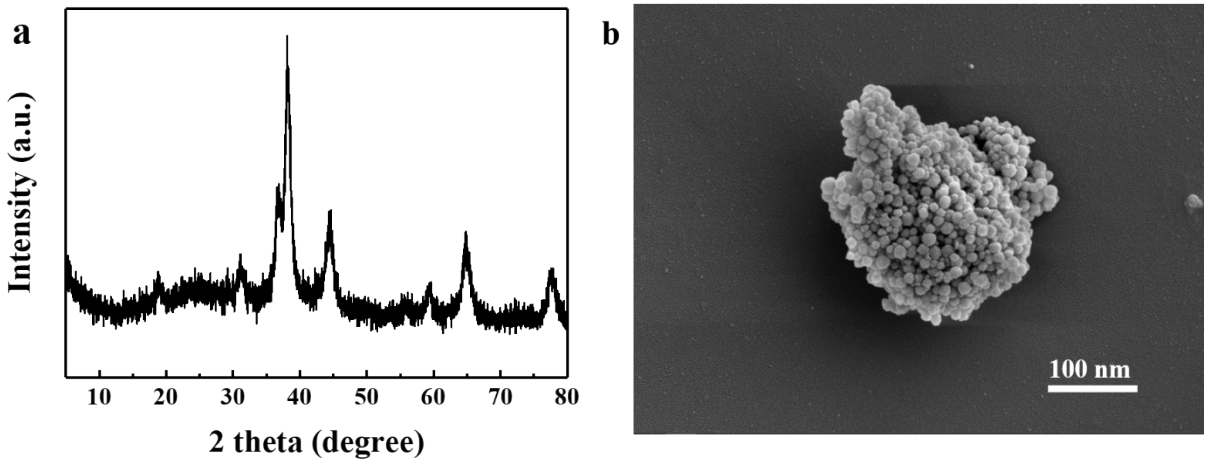

Fig. S14. XRD pattern (a) and SEM image (b) of Au@Co_3O_4 nanocomposite after catalytic reaction.

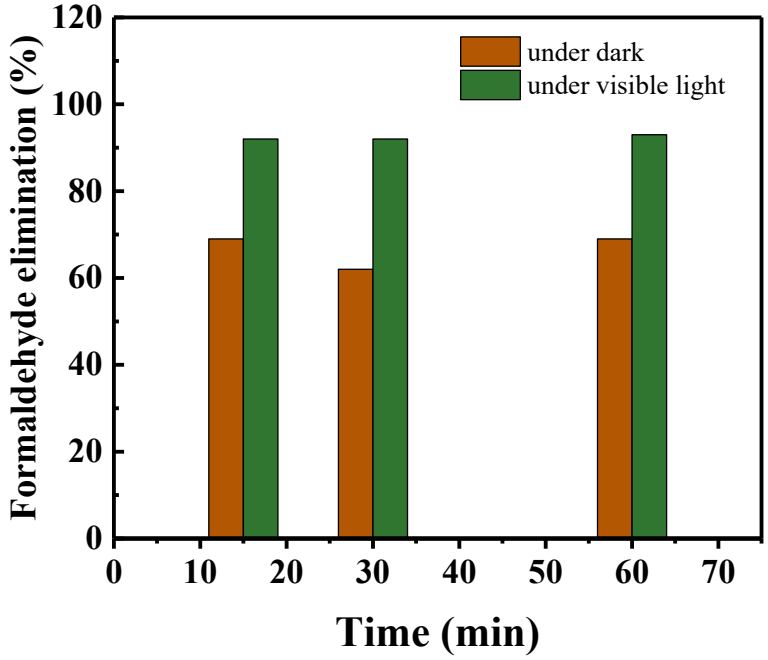

Fig. S15. Formaldehyde elimination efficiency both in the dark and visible-light irradiation at the low concentration of formaldehyde (1 ppm) in the simulate actual indoor conditions (RH 45%).

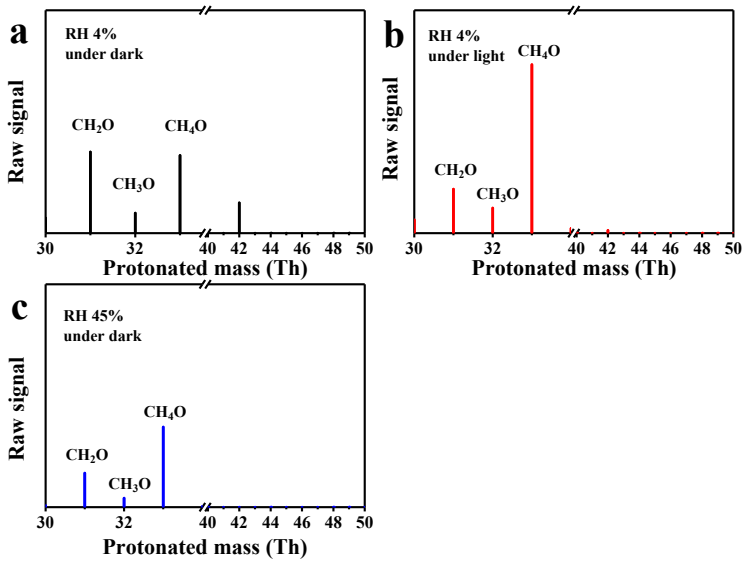

Fig. S16. PTR-QMS mass spectra with formaldehyde elimination in the dark and visible-light irradiation over Au@Co_3O_4 nanocomposite. (The tail gas collected via gas bag and diluted with nitrogen, followed by pumped into PTR-QMS)

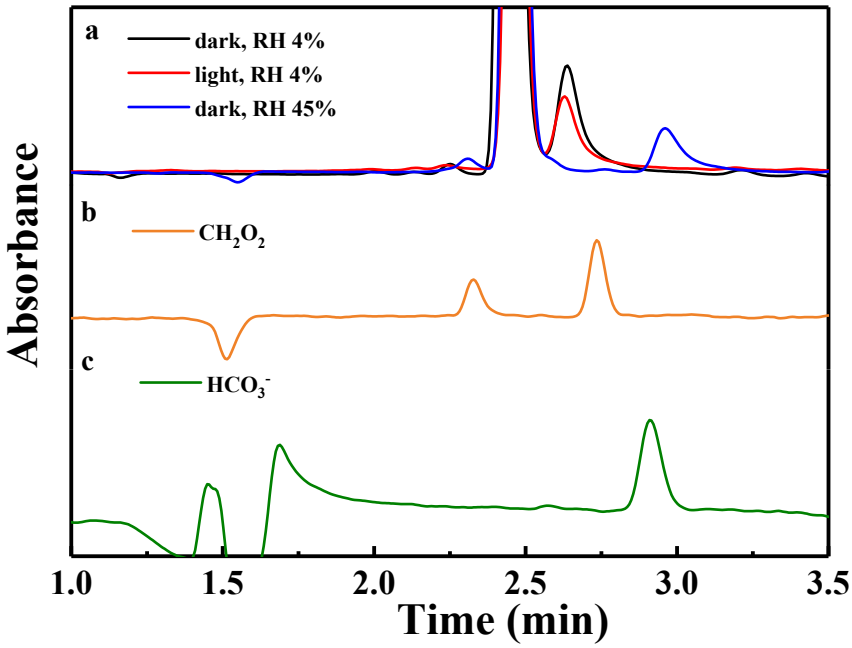

Fig. S17. HPLC chromatogram of the intermediate byproducts of formaldehyde under different conditions (a), CH_2O_2 (b), and $NaHCO_3$ (c).

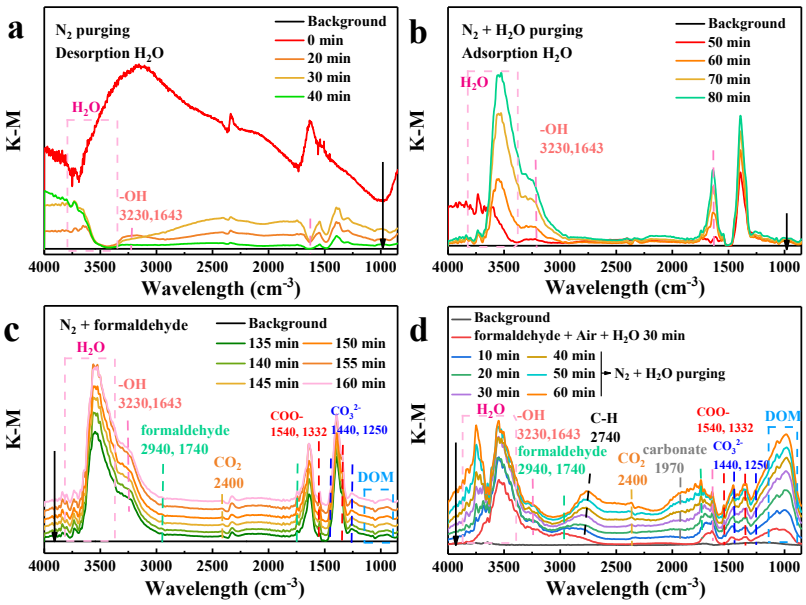

Fig. S18. Dynamic changes of *in situ* DRIFTS of Au@Co_3O_4 nanocomposite in different conditions, dehydration with N_2 purging at 120 °C (a), adsorption and activated H_2O at 30 °C (b), adsorption or elimination of formaldehyde after adsorption and activated H_2O at 30 °C (c) and N_2 + H_2O purging after elimination of formaldehyde at RH 45%, 30 °C.

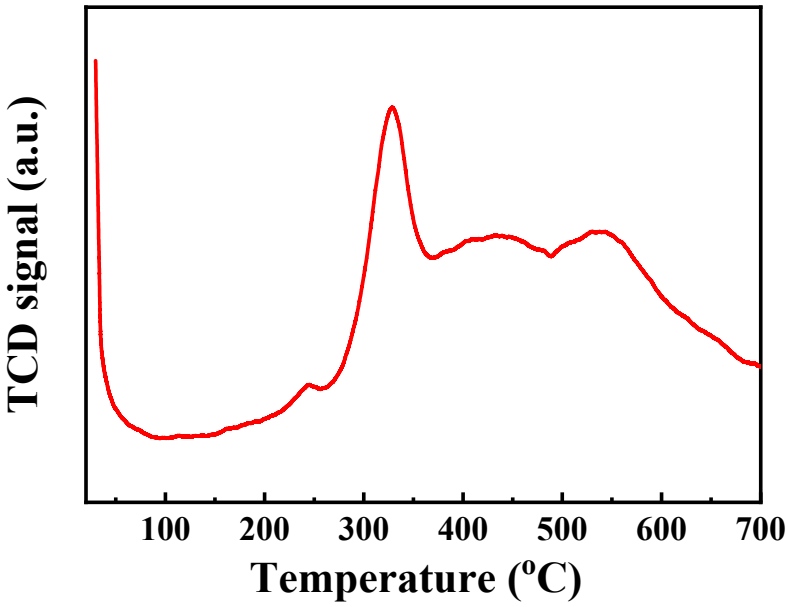

Fig. S19. O_2-TPD profiles of Au@Co_3O_4 nanocomposite (Au@Co_3O_4 adsorbed oxygen under light).

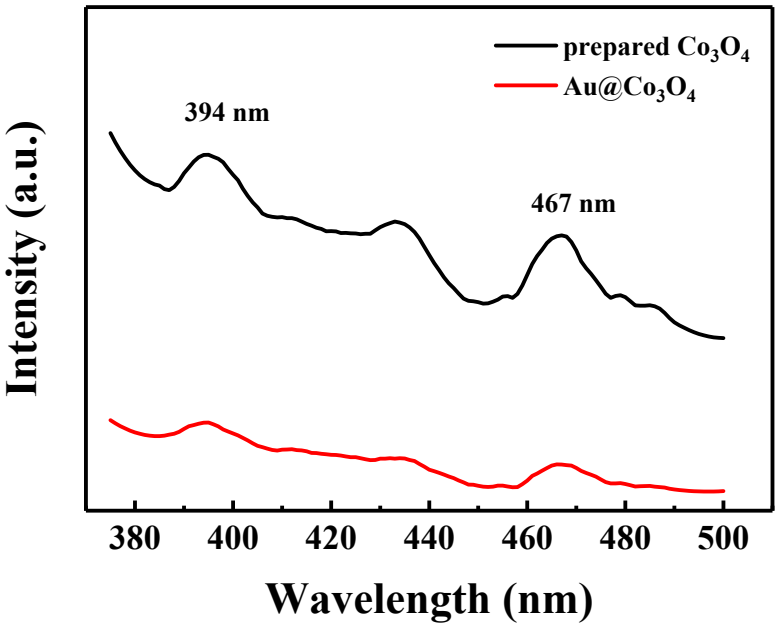

Fig. S20. PL spectra of prepared Co_3O_4 and Au@Co_3O_4 nanocomposition.

References

1. Z. Yan, N. Wang, M. Zhang, M. Xiang and Z. Xu, Indoor light boosted formaldehyde abatement over electrostatic self-assembled graphitic carbon nitride/ceric oxide at ambient temperature, *Journal of Environmental Chemical Engineering*, 2021, **9**, 106174.
2. G. Huang, Z.-H. Xu, T.-T. Luo, Z.-X. Yan and M. Zhang, Fluorescent light enhanced graphitic carbon nitride/ceria with ultralow-content platinum catalyst for oxidative decomposition of formaldehyde at ambient temperature, *Rare Metals*, 2021, **40**, 3135-3146.
3. J. Wang, X. Xu and Y. Shen, Constructing S-scheme CeO2/CN heterojunction for high efficiency light-induced photothermal synergistic catalytic degradation of gaseous formaldehyde under visible light irradiation, *Journal of Environmental Chemical Engineering*, 2022, **10**, 107436.
4. H. Wang, X. a. Dong, R. Tang, J. Li, Y. Sun, Z. Wang, K.-H. Kim and F. Dong, Selective breakage of CH bonds in the key oxidation intermediates of gaseous formaldehyde on self-doped CaSn(OH)6 cubes for safe and efficient photocatalysis, *Applied Catalysis B: Environmental*, 2020, **277**, 119214.
5. M. Ran, W. Cui, K. Li, L. Chen, Y. Zhang, F. Dong and Y. Sun, Light-Induced Dynamic Stability of Oxygen Vacancies in BiSbO4 for Efficient Photocatalytic Formaldehyde Degradation, *Energy & Environmental Materials*, 2022, **5**, 305-312.
6. Y. Wang, P. Gao, B. Li, Z. Yin, L. Feng, Y. Liu, Z. Du and L. Zhang, Enhanced photocatalytic performance of visible-light-driven CuOx/TiO2-x for degradation of gaseous formaldehyde: Roles of oxygen vacancies and nano copper oxides, *Chemosphere*, 2022, **291**, 133007.
7. Y. Huang, B. Long, M. Tang, Z. Rui, M.-S. Balogun, Y. Tong and H. Ji, Bifunctional catalytic material: An ultrastable and high-performance surface defect CeO2 nanosheets for formaldehyde thermal oxidation and photocatalytic oxidation, *Applied Catalysis B: Environmental*, 2016, **181**, 779-787.